STScI | SPACE TELESCOPE SCIENCE INSTITUTE

Instrument Science Report STIS 2021-02

STIS MAMAs: Checking for Gain Sag

Matthew T. Maclay[1]

[1]Space Telescope Science Institute, Baltimore, MD

June 3, 2021

Abstract

We present results from several tests to determine the existence and extent of gain sag in the HST/STIS MAMA detectors. By comparing the flat field response of detector regions that have experienced 2 sigma above the median cumulative count values to detector regions that have experienced the median, we aim to resolve any correlation between regional detector sensitivity and total number of counts. Additionally, we discuss fold test analysis results and discuss the ability of the fold test to detect problem pixels. We find no evidence that either the FUV or NUV MAMA detectors are experiencing global or local gain sag. We recommend further in-depth, cycle-by-cycle analysis of the flats.

Contents

1 Introduction and Background

The Multi-Anode Microchannel Array (MAMA) detectors in the Space Telescope Imaging Spectrograph (STIS) provide unique ultraviolet (UV) capabilities for high resolution spectroscopy, imaging, and coronagraphy. In a very general overview, the MAMAs consist of an entrance window, a photocathode, a curved microchannel plate (MCP), and an anode array (Woodgate et al., 1998). Figure 1 shows a diagram of these MAMA components.

Incident photons are converted to electrons at the photocathode and subsequently accelerated by an applied voltage into the MCP which has secondary emitting properties, and generates a nominal charge cloud (gain) of 7×10^5 electrons at the anode array (Woodgate et al., 1998).

The MCP's secondary emitting surface properties allow for individual photons to become detections. The rate of the secondary emission (number of electrons emitted per incident photon) and the subsequent amount of electrons that reach the detector, is the true gain of the detector. This gain is a function of the material properties in the MCP, and these properties can change over time. Overexposure can lead to degradation.

Stringent bright object protection limits and myriad safe observing practices are followed to ensure the longevity and function of the MAMA detectors. However, actual brightness thresholds and limits at which detector breakdown might occur have not been determined experimentally with MAMA detectors, since they are limited resources (B. Clampin, 1997). We present analysis on how microchannel plate detectors function after 20+ years of space-based operation and accumulated detection. It is our goal in this study to present analysis and review of the state of the STIS MAMA detectors and to ensure STIS safe observation

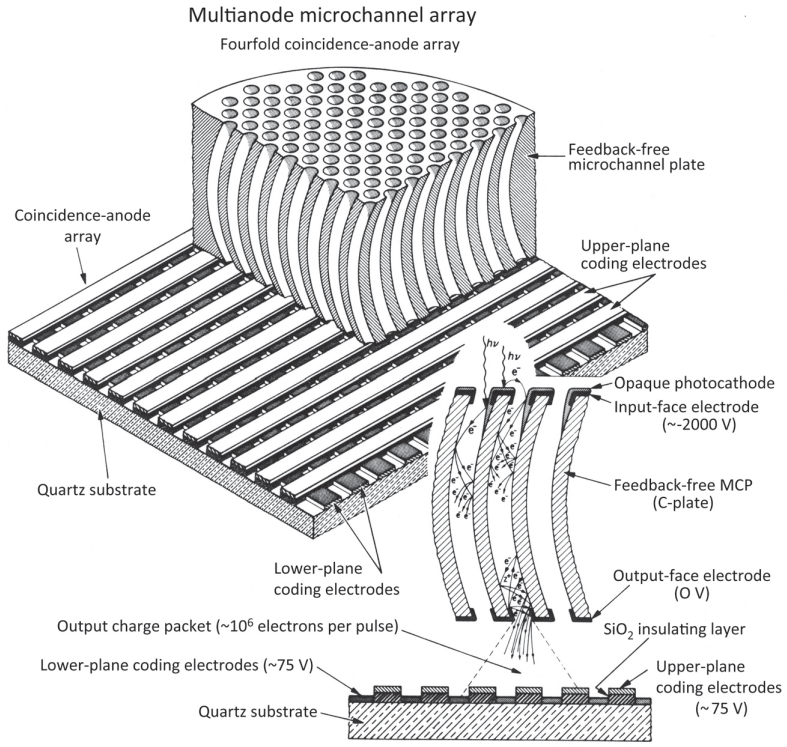

Figure 1: A schematic of the MAMA, highlighting the C-shape of the Micro Channel Plate (MCP). Photons enter the top of the MCP, and are secondarily emitted to electrons when they hit the MCP material. Figure from Timothy (2016).

practices remain effective in preventing gain sag. For a thorough and excellent review of MAMA detectors, see Timothy (2016).

1.1 Expectations

MAMA detectors can have different MCP designs, two examples being a chevron type and the C-plate type. The chevron type approximates a curve by adjoining 2 straight channel groups at an angle, while the C-plate type is an actual curved channel group. The STIS MAMAs both use a curved C-plate MCP (Fig. 1), increasing their expected longevity compared to the backup 2-plate chevron MCP. The curved channels mitigate the effects of electrons migrating backwards through the channel and hitting the photo-cathode. This results in the C-plate detectors requiring lower voltages than chevron plates to operate and being more resilient to gain changes from overexposure (Woodgate et al., 1998). This increased durability is one reason why STIS MAMAs do not have "lifetime positions" as the COS FUV XDL detector does.

While more durable than the chevron type MCP (as is used on COS FUV XDL detector), the STIS MAMAs still have stringent bright object protection limits, and exhaustive conditions set on what count rates and targets they may safely observe. In short, we have no expectation of gain sag in the STIS MAMAs with careful and normal use, but it is a possibility, and a likely outcome in the case of overexposure. Upon over-illumination, the MCP channels can experience a reduction in vacuum pressure, as the walls electrically break

down and liberate significant amounts of gas. This is expected to occur in cases where the detector is severely over-illuminated across a large fraction of its active area.

Overall the expected lifetime and durability of the MAMAs is long. Walsh et al. (1998) wrote that "The usually quoted lifetime count limit for a STIS MAMA pixel is 5×10^7 counts although the exact number depends on the individual detector." Using this number as an estimate, we can compare the count levels the detectors have captured. We estimate that the overwhelming majority of both NUV and FUV pixels have recorded less than 2% of 5×10^7 counts. Despite the long history and frequent use of STIS, we expect the detectors have the capability to continue performing excellent science for many more years.

1.2 Regular Checks for Global Gain Sag

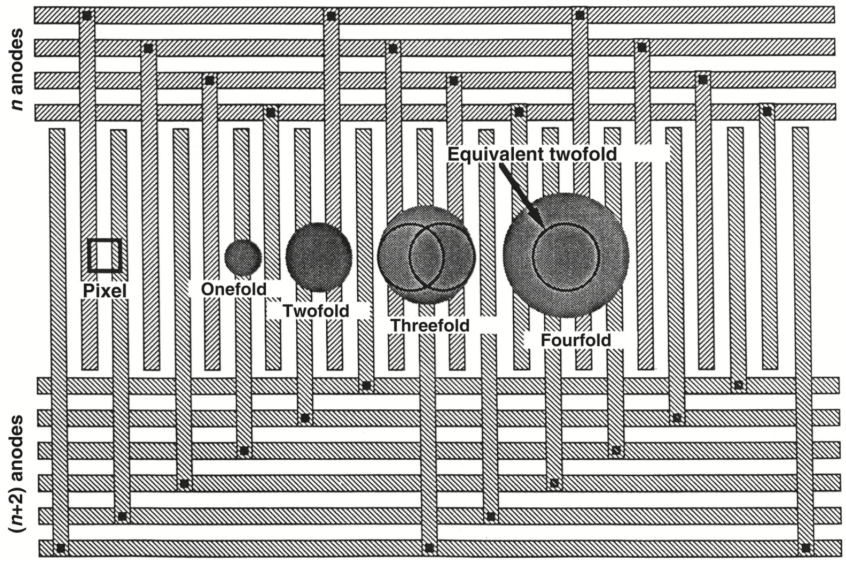

Figure 2: The size of the charge cloud detected, and the number of anodes it intersects, determines the fold number. Figure from Timothy (2016).

This report is not the first evaluation of the STIS MAMAs' gain. The MAMAs have been monitored for global changes in performance throughout their history, and risk mitigation strategies have been implemented with intentions of guaranteeing their continued and safe use.

One test that has been executed at least yearly is the fold test. In order to ensure that the detectors are not experiencing a significant decrease in gain, a fold test is conducted every cycle (15754, 15565, 14976, etc., PI: Tom Wheeler).

The fold test is a cumulative test wherein the MAMA in question is exposed to incident photons from a STIS lamp, and the detector counts how large the measured charge clouds are, albeit with **no** spatial or pixel information recorded. Figure 2 shows how fold value is determined based on charge cloud size. The fold number is determined by the size of the incident electron cloud, particularly how many anodes it intersects. Given that the gain determines the size of the charge cloud, decreasing fold numbers would indicate a large scale decrease in detector gain.

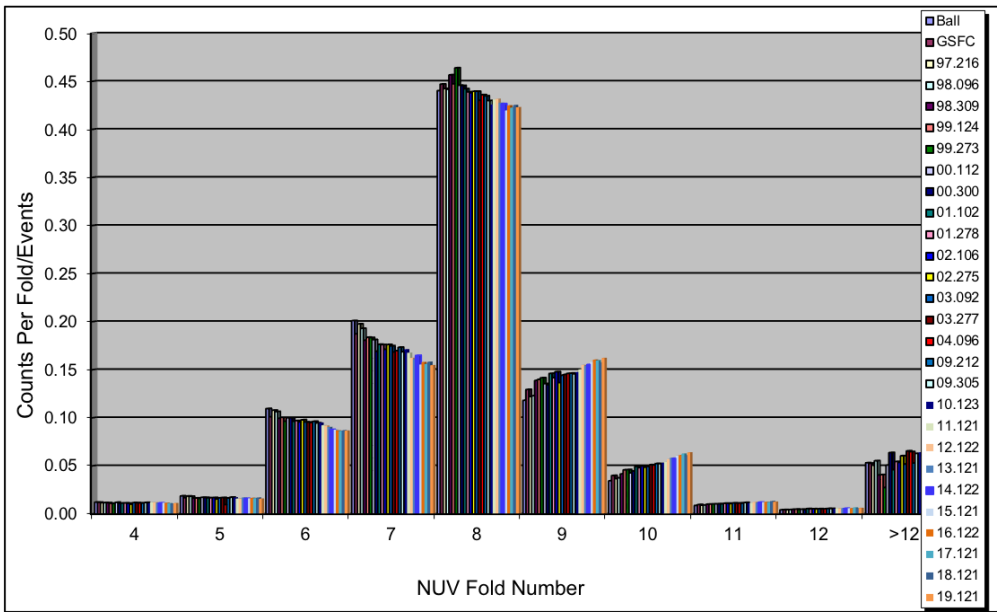

Figure 3: The NUV fold test results from 1997 - 2019. The fold number represents the size of the charge cloud detected, and each set of same-color columns is a measurement from a specific year. We see that the NUV fold numbers have become more normally distributed around a fold value of 8 (most recent data in orange). We see no increase in low fold number occurrences, suggesting no detector-wide issues. Figure from Tom Wheeler (private communication, 2019)

The fold test utilizes a special detector mode that records distributions of charge cloud size and does not record the x,y positions of the events. This test is designed as a quick way to make sure there are no big problems with the detector gain that would show up in the frequency distributions of measured charge cloud size. Because it lacks spatial information, this test is *very unlikely* to resolve small-scale or localized gain sag (Tom Wheeler, private communication).

Figures 3 and 4 show fold test results from 1997 to 2019 for the NUV and FUV MAMAs, respectively (Tom Wheeler, Private communication). Both figures show count distributions of fold number (a proxy for global detector gain) over time, with each set of same-color columns representing a given cycle. In the NUV fold test, we see no negative trends in the charge cloud size distributions over time. If anything, the distribution seems to have moved more positive; we see a decrease in 7 and an increase in 9. In the FUV fold test, we see no negative trend over time, but a decrease in 8 and an increase in 10.

The fold test is a rough analysis that allows us to check for global or drastic degradation of detector capability. In both fold distributions, we see a slight positive trend in fold number over time, indicating that the average charge cloud size recorded is slightly greater than earlier in the instrument's life. This behavior is the opposite of global gain sag characteristics. A systematic shift toward lower fold values would be indicative of a loss of gain in the MCP, while an increase in saturated pulses might suggest "gassiness" in the tube (Kimble et al., 1999). The instrument scientist (V. Argabright) formerly at Ball Aerospace has indicated that small positive fold value trends are not a cause for concern (Tom Wheeler, private communication).

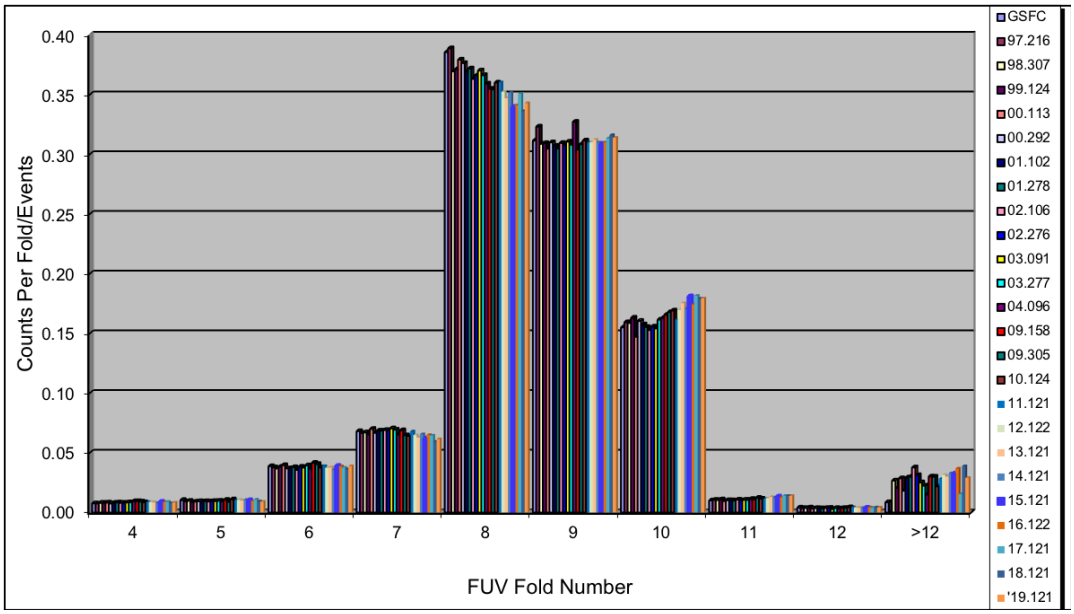

Figure 4: The FUV fold test results from 1997 - 2019. The fold test is a rough analysis that allows us to check for global or drastic degradation of detector capability. Each color represents the distribution from a different year - allowing the reader to discern any trends in the distribution over time. Figure from Tom Wheeler (private communication, 2019)

2 Looking for Local Gain Sag

The fold test is an excellent tool to rapidly take a snapshot of the global health of the MAMA detectors, but it does not retain any spatial information (i.e. where on the detector low or high fold values are occurring). Because the STIS MAMAs are so frequently used in their spectroscopic (echelle and long slit) capacity, there are specific areas of the detector that have experienced much more incident light than others throughout the history of the instrument.

It is quite likely that the fold test would not resolve a small group of pixels that have much lower sensitivities due to gain sag. For example, if one or two rows were suffering from severe gain sag, the fold distribution would not make that apparent. For this reason, we aim to check if regions of high use have different gain behavior than regions of lower usage. In order to determine this we use cumulative count image (CCI) files.

2.1 Cumulative Images as a Map of Detector History

Each CCI file is the integration of all exposures for a given detector over an approximately weekly (9 day) time period. They are generated in the calibration pipeline, and can be retrieved via a sql query. By superimposing all of the files since 2009, we see where on the FUV and NUV MAMAs the highest and lowest use pixels are.

Using the CCI files, we can identify which pixels have detected significantly more than the average number of counts, and test if those groups demonstrate different gain behavior in the flat field (which measures sensitivity). It is important to note that the cumulative images are not perfect maps that describe which pixels have had the most counts. Any

intrinsically unresponsive or bad pixels will appear to register fewer historical counts in the cumulative images regardless of how many incident electrons there actually were. These cumulative images are also subject to problem pixels and sensitivity issues, so it is impossible to perfectly resolve the exact number of counts registered from the intrinsic response of the detector.

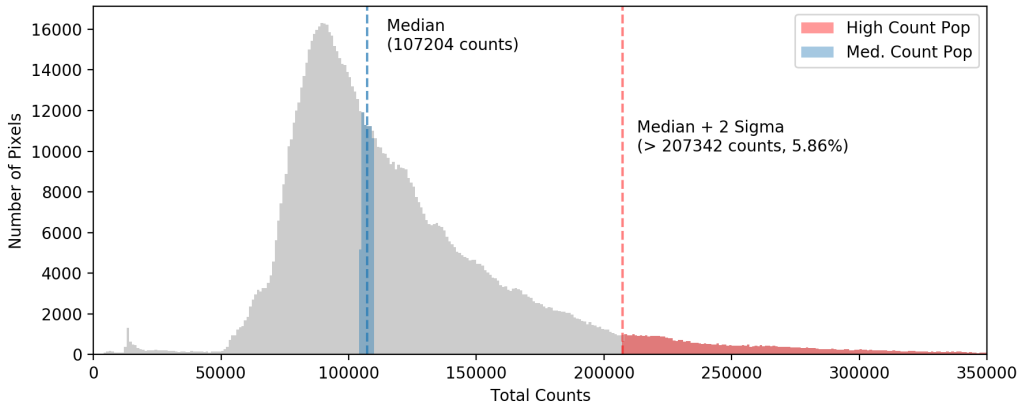

(a) NUV Distribution

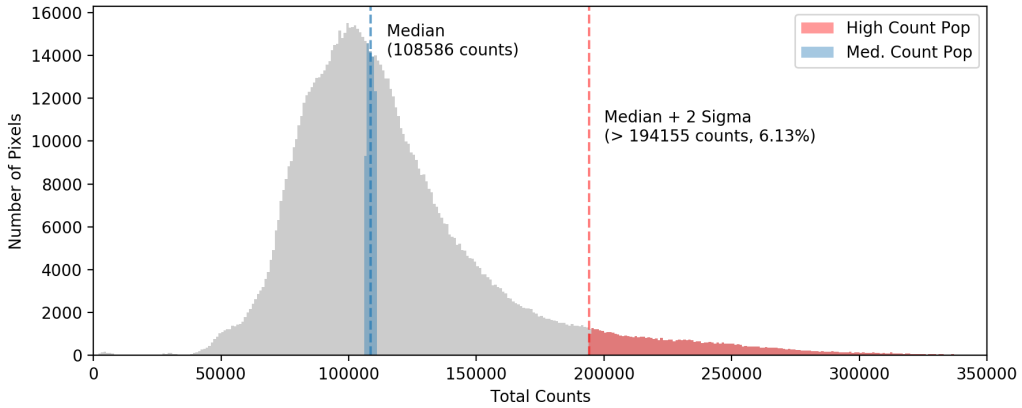

(b) FUV Distribution

Figure 5: The distribution of counts registered in the last 10 years (2009-2020) for the NUV and FUV detectors. We have identified the pixels that have received 2 sigma more counts than the median number of counts for each detector (shown in red) and an equally sized population centered on the median (shown in blue). (5a): Distribution of count values in the post-SM4 cumulative images for the NUV MAMA. Note the low count bump around 20000 counts, likely due to the vignetting in the corners of the detector. (5b): Distribution of count values in the post-SM4 cumulative images for the FUV MAMA.

2.2 Choosing Pixel Populations

Using CCI files, we can construct a picture of where the MAMA detectors have experienced the most incident electrons in their history. We can directly compare the flat field response of pixels in high-use and low-use regions of the detector in order to determine if there is any count-history correlation with gain sag.

For each detector, we created equally sized high-count and a median-count populations of pixels. The high-count population consists of all pixels that have received 2 standard deviations more than the median number of counts ($\approx 6\%$ of all pixels). The median-count population contains the same number of pixels as the high-count group but centered around the median count value, such that all the pixels are essentially at the median value. We use the same number of pixels in each group to simplify statistical comparisons.

Population	**Count Percentiles**	**# Pixels**
High-Count ($>2\sigma$)	94.14 - 100%	61488
Median-Count	47.07 - 52.93%	61488

Table 1: NUV/MAMA detector population values using all counts from 2009-2020.

Population	**Count Percentiles**	**# Pixels**
High-Count ($>2\sigma$)	93.87 - 100%	64285
Median-Count	46.935 - 53.065%	64285

Table 2: FUV/MAMA detector population values using all counts from 2009-2020.

Figures 5a and 5b visualize high-count and median-count populations in the distribution of counts detected by all pixels from 2009-2020 for the NUV and FUV MAMAs. Tables 1 and 2 further specify the extracted population percentiles and sizes.

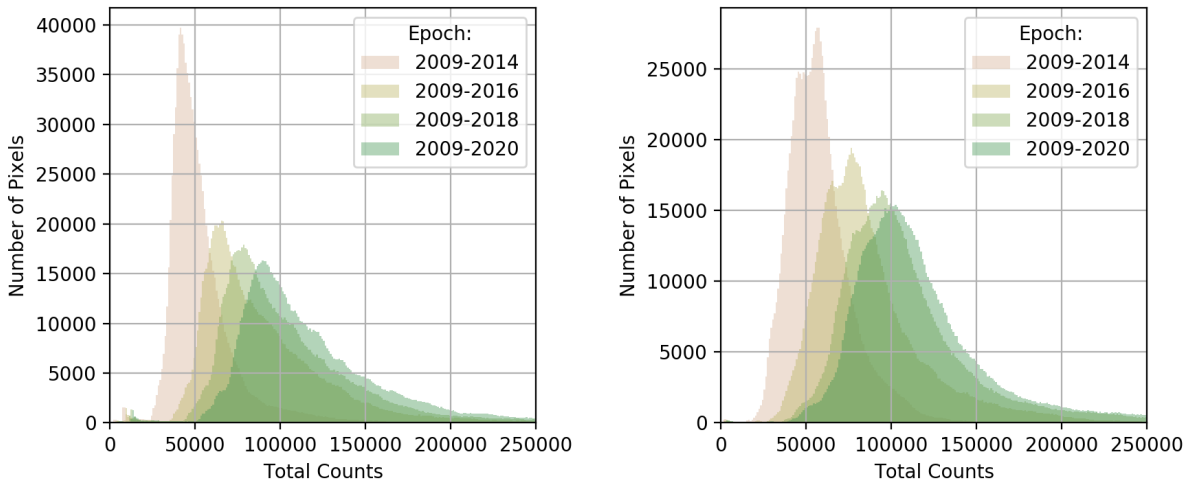

(a) NUV Distribution **(b)** FUV Distribution

Figure 6: Count distributions over time. Both the NUV and FUV are right-skewed distributions. (6a): The distribution of counts registered by the NUV detector over time. We see that the distribution started very right skewed, and is slightly less right skewed as of 2020. (6b): The distribution of counts registered by the FUV detector over time. We see that the distribution began with a double peak, and has since become more normal. It is possible the second peak is due to the FUV flow region.

The NUV distribution is noticeably sharper and more right skewed than the FUV distribution, which is closer to normal. In order to determine if this sharpness is increasing

over time, and determine if the differences in cumulative (2009-2020) distributions of the NUV and FUV MAMAs are changing, we examine how these cumulative distributions have evolved over time. Figure 6 shows the cumulative count distributions over time for the NUV and FUV detectors. Starting with the first 5 years after SM4, and including 2 more years of use with each epoch, Figure 6 shows that both the NUV and FUV distributions have become more normal with increased use. Initial distributions were sharper and more right-skewed, but we see for both detectors the distributions have become broader and smoother. As an example, the FUV distribution had a double peak in the early epoch and this has been smoothed over since, suggesting that the cause was likely low count statistics and there are no apparent concerning trends developing. This is reassuring, because new changes in detector sensitivity might cause a distribution to suddenly become sharper, bi-modal, or less normal over time.

2.3 Comparing Population Sensitivity in the Flat Field

In order to compare the sensitivities of the median-count and high-count populations, and measure their values in the most recent available (Cycle 26) FUV superflat and (Cycle 25) NUV superflat, we compare the measured values of the extracted pixels in the flat field. We aim to find any correlation between the historical count value with the measured flat field sensitivity. Figure 7 shows the NUV cumulative count images, extracted pixel populations, and cycle 25 NUV superflat. Figure 8 shows the FUV cumulative count populations, extracted pixel populations, and cycle 26 FUV superflat.

As described in the previous section, we determine the populations of pixels by selecting pixels that have the median and $> 2\sigma$ above the median number of registered counts in the detector's cumulative history. We then measure the values of those same pixels in the flat, to see if there are any correlations between pixel usage history and current flat sensitivity. We are testing for this correlation because we might expect that pixels which have experienced many more incident counts throughout detector history (eg. the spectral orders in the CCI images), are most likely to have decreased flat field response due to gain sag.

3 Results

Figure 9 shows the actual flat field count values of the median-count and high-count pixel populations for the NUV and FUV MAMA detectors. We see in both detectors that the high and median count distributions are narrow and largely overlapping in their flat field values, indicating overall uniform detector sensitivity.

Severe local gain sag would correspond to the high count population being significantly lower in flat field sensitivity than the median-count population. We find nothing that suggests a sag in the gain of either detector, from these distributions.

3.1 NUV Population Comparison

In the NUV, (Figure 9a) the pixels in the high count population are slightly less responsive in the Cycle 25 median NUV flat than the pixels in the median-count population. We can

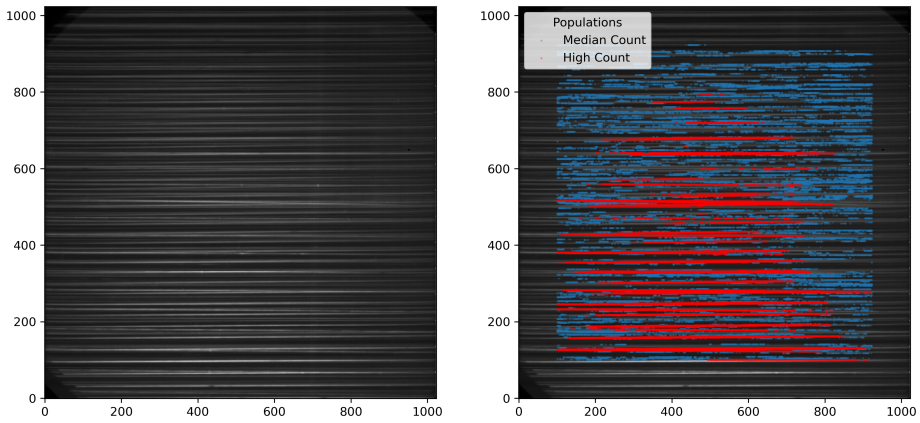

(a) NUV CCI **(b)** NUV CCI & Pixels

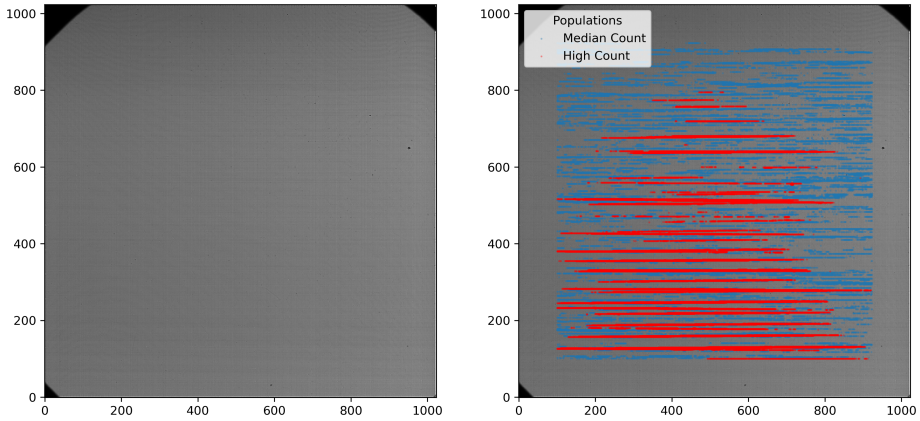

(c) NUV Flat **(d)** NUV Flat & Pixels

Figure 7: Visual representation of extracting populations from the CCI and comparisons to the flat field image for the NUV. (7a): The cumulative, post-SM4, image of STIS NUV data. We can see various spectral orders from the echelle and long slit gratings (brighter in white). (7b): The cumulative, post-SM4, image of STIS NUV data with the high and median count extracted populations overlaid. (7c): The Cycle 25 NUV flat. This is a median combined image that is designed to be a uniform projection onto the detector. Note the vignetting in the corners. (7d): The Cycle 25 NUV flat with the high and median count populations overlaid.

perform a statistical difference of means analysis using the distributions' means, standard deviations, and number of samples. We find with 95% confidence, pixels in the high-count population are 0.28 - 0.42% less sensitive than median pixels in the NUV flat. While this is in the direction of potential gain sag, it is not a significant amount, and does not indicate notable gain sag in the NUV detector.

3.2 FUV Population Comparison

In the FUV, (Figure 9b) pixels in the high-count population of incident electrons are actually more responsive in the Cycle 26 median FUV flat than the pixels in the median-count population. We perform an equivalent statistical analysis to the NUV population. With

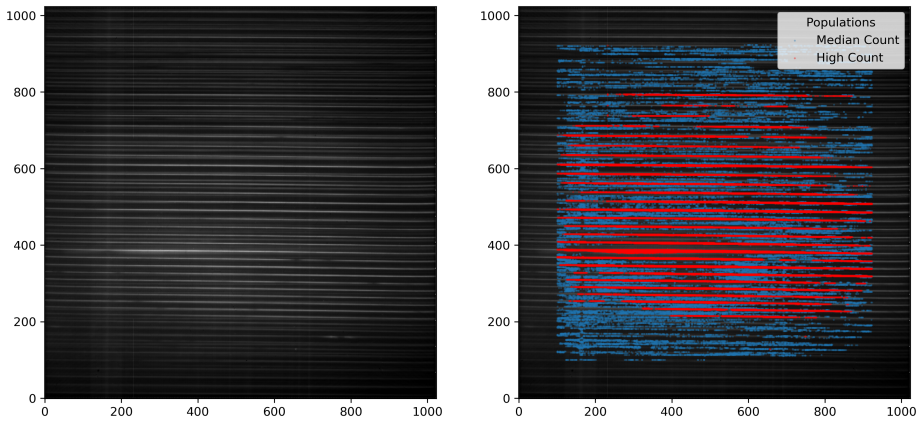

(a) FUV CCI **(b)** FUV CCI & Pixels

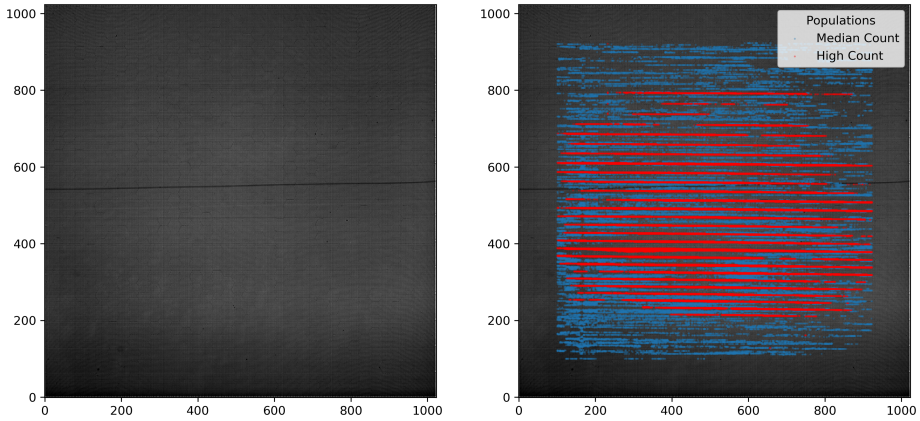

(c) FUV Flat **(d)** FUV Flat & Pixels

Figure 8: Visual representation of extracting populations from the CCI and comparisons to the Flat for the FUV. (8a): The cumulative, post-SM4, image of STIS FUV data. (8b): FUV CCI with the high and median count populations overlaid. (8c): The Cycle 26 FUV flat. (8d): The Cycle 26 FUV flat with the high and median count populations overlaid.

95% confidence, pixels in high-count population are 3.9 - 4.1% more sensitive than median pixels in the FUV flat. These pixels seem to have behavior that resembles stable hot-pixels. We discuss the nature of this positive correlation further in Section 3.3. There is no indication of gain sag in the FUV MAMA.

3.3 Checking All Pixels

This statistical comparison suggests that bright object protection limits and careful safe practices have been largely effective at preventing gain sag. The results also do not suggest any gain dependence on total counts, and confirm the overall resiliency of the MAMAs. However, this does not rule out the possibility of any and all gain sag. In directly comparing populations of pixels based on their cumulative incident photons, we have explicitly examined the effect of cumulative counts (not count rates) on individual pixels. Overall, we find that a

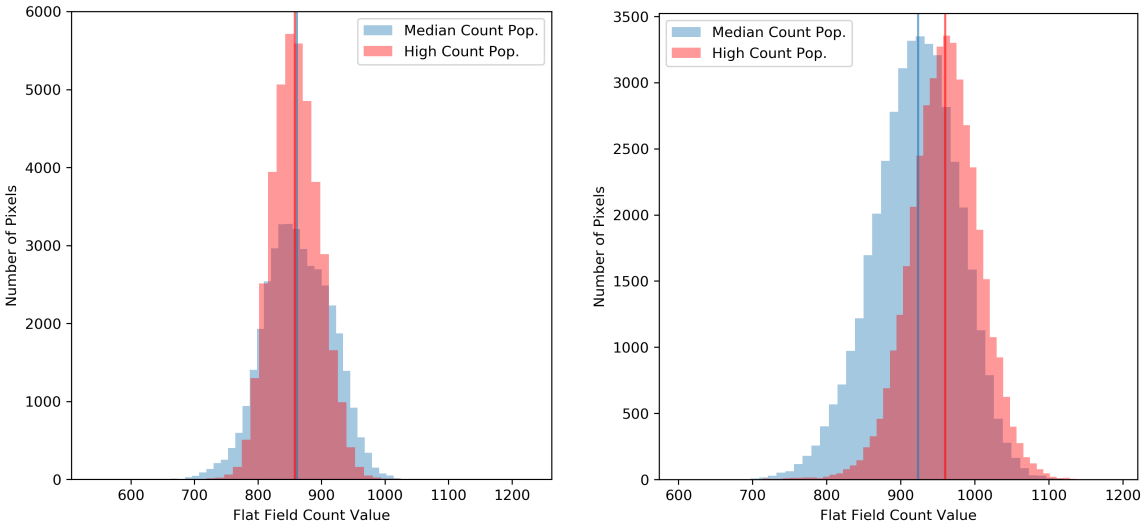

(a) NUV Distribution **(b)** FUV Distribution

Figure 9: Flat field sensitivity distributions of high and median count populations. (9a): The high and median count populations are almost entirely overlapping for the NUV detector. With 95% confidence, pixels in the high count population are 0.28-0.42% less sensitive in the NUV flat. (9b): The high-count population is slightly more sensitive than the low count for the FUV detector. With 95% confidence, pixels in the high-count population are 3.9-4.1% more sensitive in the FUV flat. This is the opposite of the expected effect of gain sag, and we discuss this in Section 3.3.

pixel's recorded cumulative counts is not predictive of the pixel's apparent gain performance.

Our above conclusions are further supported when we look at Figures 10a and 10b, where we plot every pixel's flat field response against how many counts it has historically registered. There are a few distinct groups of pixels that correspond to nonstandard behaviors (eg. problem pixels, hot-pixels, etc.) but the overwhelming majority of pixels follow a uniform horizontal trend with consistent flat field sensitivity.

While the majority of pixels are at a uniform flat field value (y $\approx$ 1000 counts) regardless of cumulative counts, both plots in Figure 10 have a small number of pixels with a positive linear correlation (pixels spanning from the origin to about $x \approx 200000, y \approx 2000$). This behavior resembles stable hot-pixels and effects both the CCIs and the flats. Since, over time, more sensitive pixels will register more counts, and less sensitive pixels will register fewer counts, this group of pixels shows a positive correlation between the cumulative counts and sensitivity measured in the flat. The inclusion of these pixels in the high-count populations also supports the results in the statistical test, where the high-count population is actually more sensitive in the flat than the median-count population.

In Figure 10a, there are some pixels that do not follow the correlation trend, yet seem to have a higher flat field level. These pixels seem to have a very slight correlation or perhaps even a constant flat field sensitivity offset. This behavior resembles what we expect from hot-pixels. Despite these hot-pixels, the high-count population (red) distribution is centered on 850 counts in the flat, and is less populous in higher flat field values.

In Figure 10b, we see that pixels that do not follow the main horizontal trend are part of the positive correlation trend. This suggests that most of the hot-pixels on the FUV/MAMA

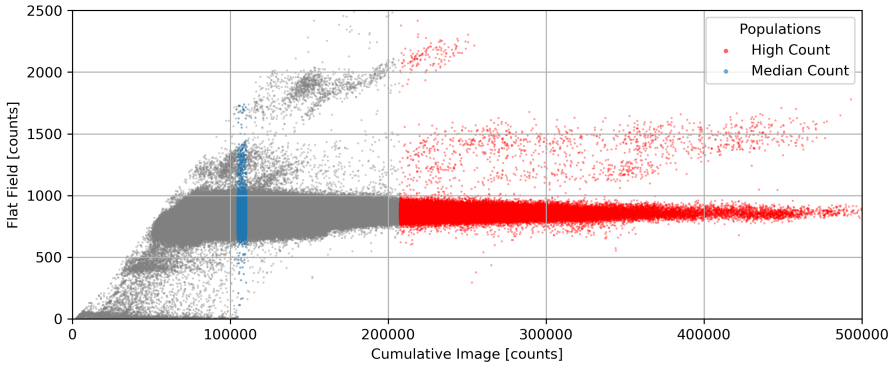

(a) NUV Pixels

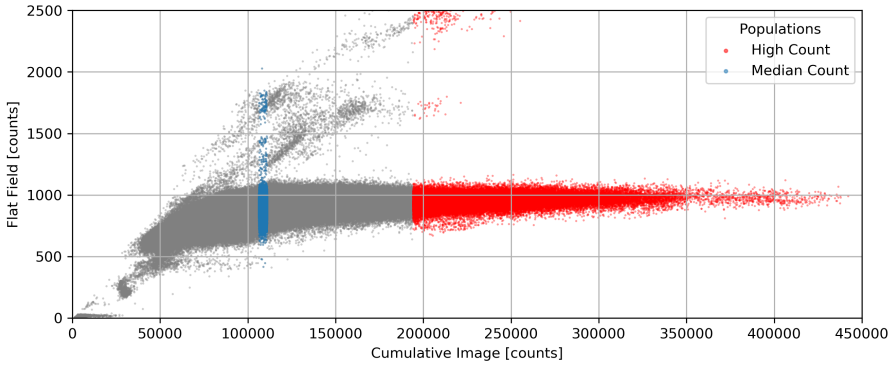

(b) FUV Pixels

Figure 10: The value of each pixel in the flat field is plotted against recorded cumulative counts in the last 10 years. We have identified the pixels that have received 2 sigma more counts than the median number of counts for each detector (in red) and an equally sized population centered on the median (in blue). (10a): Flat field sensitivity of each NUV MAMA pixel plotted as a function of cumulative recorded counts. There appears to be a slight dip in the flat values in pixels above $\approx$300000 counts, but this is only a perceived effect as the sample size decreases, and the center of the distribution is revealed. (10b): Flat field sensitivity of each FUV MAMA pixel plotted as a function of cumulative recorded counts. We see good stability in the flat field sensitivity even in the highest count regimes.

have responses that scale with counts, and few simply do not scale.

Our samples in Figure 9 are consistent with the broader detector-wide results shown in Figure 10. The overwhelming majority of the pixels have a consistent flat field sensitivity that is not dependent on historical counts. There is no negative correlation between a pixel's historical counts and flat field sensitivity which would indicate gain sag.

4 Conclusions and Discussion

The STIS MAMAs continue to perform nominally, and we expect them to continue. The overwhelming majority of both NUV and FUV pixels have recorded less than 2% of 5×10^7 counts, which is their approximate life-expectancy. We expect the detectors to gather many more counts and perform excellent science for many more years.

We see no evidence of gain sag from our cumulative count tests and we look forward to a

bright future with STIS. We can safely rule out large global gain sag in both the NUV and FUV MAMAs. We also find that there does not appear to be a clear correlation between cumulative counts and pixel gain.

This result supports what was believed to be the case, that curved C-plate MCPs are more resilient than the chevron type MCPs (B. Clampin, 1997 & Woodgate et al., 1998), and provides a current update to a long detector history. Additionally, our current count values for the detector are believed to be under 2% of their expected total count lifetimes (Walsh et al., 1998).

4.1 Discussion

In-depth, pixel-by-pixel analysis is important, as other regular tests (the fold test) are unlikely to detect localized gain sag. Additionally, the majority of STIS science data are incident with a small fraction of the total detector, so even a local issue would be a problem. This work points us to a clear next step for further investigation. In this report, our methods focus on total historical counts of the detector, and not on specific observation periods with local and global count rate analysis. Gain sag could certainly be caused by extremely high count rates observed for only a short amount of time. This is a good topic for future analysis. While cumulative counts do not have any clear correlation with detector gain performance, count rates may be more indicative of time-dependent trends, as suggested in literature (B. Clampin, 1997).

We keep in mind that intrinsically unresponsive or bad pixels will appear to register fewer historical counts in the cumulative images, thus it is impossible to truly know the number of counts historically incident on the detector, because the intrinsic pixel sensitivity of the pixels (measured via the flat) impacts the CCI files.

4.2 Future Work

The next step is an in-depth flat field analysis, particularly an analysis of how the MAMA flats have evolved over time. During the course of this flat field investigation, it would be interesting to utilize the CCI files to compare how the CCI and flat field changed over the same time periods.

The evolution of the MAMA flats over time will be an interesting and useful analysis on its own, and we anticipate that incorporating cycle by cycle correlation with the CCI files may yield further insights. Higher time resolution (i.e. a cycle-to-cycle comparison) will allow us to resolve the direct impact of high count rates on the particular sensitivities of the detectors.

One thing that would be interesting is to look at how the plots in figure 10 may have changed over time. This could reveal if any pixels systematically migrated through that plot, i.e. changed flat field sensitivity. In order to perform this analysis, one would have to normalize the different cycle flat fields to one another as the lamp values change over time.

5 Acknowledgements

We thank David Sahnow for discussion on MAMA detectors, Thomas Wheeler for discussion on the fold test and detector history, Tony Sohn for inspiration to check the STIS CCI files, Tala Monroe and the STIS team for helpful feedback.

References

B. Clampin (May 1997). "Bright Object Protection Mechanisms for STIS". In: *STScI Instrument Science Reports*.

Kimble, Randy A. et al. (1999). "In-flight performance of the MAMA detectors on the Space Telescope Imaging Spectrograph". In: 3764. Ed. by Silvano Fineschi, Bruce E. Woodgate, and Randy A. Kimble, pp. 209–225. DOI: 10.1117/12.371085. URL: https://doi.org/10.1117/12.371085.

Timothy, J. Gethyn (2016). "Review of multianode microchannel array detector systems". In: *Journal of Astronomical Telescopes, Instruments, and Systems* 2.3, pp. 1–23. DOI: 10.1117/1.JATIS.2.3.030901. URL: https://doi.org/10.1117/1.JATIS.2.3.030901.

Walsh, J. R. et al. (Feb. 1998). "Specification and Application of the MAMA Additive Image (MADDIM) to Track Charge Extraction". In: *STScI Instrument Science Reports* 98.30.

Woodgate, B. E. et al. (Oct. 1998). "The Space Telescope Imaging Spectrograph Design". In: *Publications of the Astronomical Society of the Pacific* 110.752, pp. 1183–1204. DOI: 10.1086/316243. URL: https://doi.org/10.1086%2F316243.